# Development and Implementation of a Differential Wheel – Rail Contact Model for Multibody Applications

**S. Magheri*, M. Malvezzi**, E. Meli*, S. Papini***

* Dipartimento di Energetica
Università di Firenze
Via di S. Marta 3, 50100 Firenze, Italia
email: silvia.magheri@unifi.it, meli@mapp1.de.unifi.it,
susanna@mapp1.de.unifi.it

** Dipartimento di Ingegneria dell'Informazione
Università di Siena
Via Roma 56, 53100 Siena, Italia
email: malvezzi@dii.unisi.it

## ABSTRACT

The wheel - rail contact analysis plays a fundamental role in the multibody modeling of railway vehicles. A good contact model must provide an accurate description of the global and local contact phenomena (contact forces, position and shape of the contact patch, stresses and displacements) and a general handling of the multiple contact. The model has also to assure high numerical efficiency (in order to be implemented directly online within multibody models) and a good compatibility with commercial multibody software (Simpack Rail, Adams Rail).
In this work the authors intend to present an innovative elastic wheel - rail contact model that satisfies the previous specifics. The model considers the wheel and the rail as elastic deformable bodies and requires the numerical solution of the Navier's elasticity equation. The contact between wheel and rail has been described by means of suitable analytical contact conditions. Subsequently the contact model has been inserted within the multibody model of a benchmark railway vehicle (the Manchester Wagon) in order to obtain a complete model of the wagon. The whole model has been implemented in the Matlab environment. Finally numerical simulations of the vehicle dynamics have been carried out on many different railway tracks with the aim of evaluating the performances of the model.
In conclusion the main purpose of the authors is to achieve a better integration between the differential modeling and the multibody modeling. This kind of integration is almost absent in literature (especially in the railway field) due to the computational cost and to the memory consumption. However it is very important because only the differential modeling allows an accurate analysis of the contact problem (in terms of contact forces, position and shape of the contact patch, stresses and displacements) while the multibody modeling is currently the standard in the study of the railway dynamics.

**Keywords:** Multibody modeling, wheel – rail contact, contact between elastic bodies.

## 1 INTRODUCTION

The wheel - rail contact problem has been discussed by several authors and many models can be found in the literature. Currently the main multibody approaches to the problem are the so - called rigid contact formulation and the semi – elastic contact description. The rigid approach considers the wheel and the rail as rigid bodies. The contact is imposed by means of constraint equations and the contact points are detected during the dynamic simulation by solving the nonlinear algebraic differential equations associated to the constrained multibody system. Indentation between the bodies is not permitted and the normal contact forces are calculated through the Lagrange multipliers. Finally the Hertz's and the Kalker's theories allow to evaluate respectively the shape of the contact patch and the tangential forces. [1][2][3][4][5][6] Also the semi - elastic approach considers the wheel and the rail as rigid bodies. However in this case there are not constraints and the indentation between the bodies is permitted. The contact points are detected by means of approximated procedures (based on look - up tables and

simplifying hypotheses on the problem geometry) or by means of semi - analytical methods (based on the reduction of the problem dimension). The normal contact forces are calculated as a function of the indentation while, as in the rigid approach, the Hertz's and the Kalker's theories allow to evaluate the shape of the contact patch and the tangential forces. [4][5][6][7][8][9]
Both the described multibody approaches are computationally very efficient but their generality and accuracy turn out to be often insufficient because the physical hypotheses behind these theories are too restrictive and, in many circumstances, unverified.
In order to obtain a complete description of the contact phenomena, differential contact models are needed. In other words wheel and rail have to be considered elastic bodies governed by the Navier's equations and the contact has to be described by suitable analytical contact conditions. The contact between elastic bodies has been widely studied in literature both in the general case and in the rolling case. Many procedures based on variational inequalities, FEM techniques and convex optimization have been developed. This kind of approach assures high generality and accuracy but still needs very large computational costs and memory consumption. [4][10][11][12][13][14]
Due to the high computational load, referring to the current state of the art, the integration between multibody and differential modeling is almost absent in literature especially in the railway field. However this integration is very important because only the differential modeling allows an accurate analysis of the contact problem (in terms of contact forces, position and shape of the contact patch, stresses and displacements) while the multibody modeling is the standard in the study of the railway dynamics.
In this work an innovative differential contact model is presented with the aim of achieving a better integration between multibody and differential modeling. The new contact model is fully 3D and satisfies all the specifics described above. The developed procedure requires the discretization of the elastic contact problem (Navier's equations and analytical contact condition) and subsequently the solution of the nonlinear discrete problem. Both the steps have been implemented in Matlab environment. At this point the contact model has been inserted within a 3D multibody model of a railway vehicle to obtain a complete model of the wagon. The railway vehicle chosen as benchmark is the Manchester Wagon the physical and geometrical characteristics of which are easily available in the literature. [15] The multibody model has been implemented in SimMechanics, a Matlab toolbox specifically designed for multibody dynamics.
The 3D multibody model of the same vehicle (this time equipped with a standard contact model based on the semi - elastic approach) has been then implemented also in Simpack Rail, a commercial multibody software for railway vehicles widely tested and validated.
Finally numerical simulations of the vehicle dynamics have been carried out on many different railway tracks with the aim of evaluating the performances of the whole model. The comparison between the results obtained by the Matlab model and those obtained by the Simpack Rail model has allowed an accurate and reliable validation of the new contact model.

## 2 GENERAL ARCHITECTURE OF THE MODEL

As said in the introduction the whole model consists of two different parts: the 3D multibody model of the railway vehicle (the Manchester Wagon [15]) and the 3D differential wheel - rail contact model. The general architecture of the model is schematically shown in Figure 1.

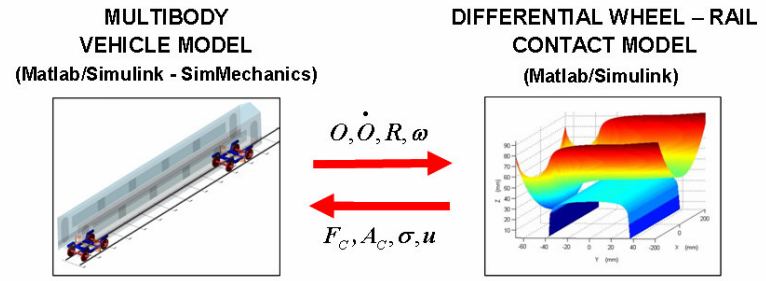


**Figure 1.** General architecture of the model.

During the simulation the multibody model interacts directly online with the differential contact model. At each time integration step the multibody model evaluates the kinematic variables relative to the wheelset and consequently to each wheel - rail contact pair. Starting from these quantities, the contact model, based on Navier's equations and suitable analytical contact conditions, calculates the global and local contact variables (forces, contact areas, stresses and displacements). Finally the knowledge of the contact variables allows the multibody model to carry on the simulation of the vehicle dynamics.

## 3 REFERENCE SYSTEMS AND RAILWAY TRACK

First of all a *fixed reference system* $O_f x_f y_f z_f$ (in which the track $\boldsymbol{\gamma}(s)$ is described) is defined (Figure 2a). Subsequently a second reference system, referred as *auxiliary reference system* $O_R x_R y_R z_R$ (Figure 2a and 2b), is introduced. It is placed on the plane of the rails and follows the motion of the wheelset during the simulation. Finally the *local reference system* $O_W x_W y_W z_W$ is defined; this system is rigidly connected to the wheelset except for the rotation around its axis.

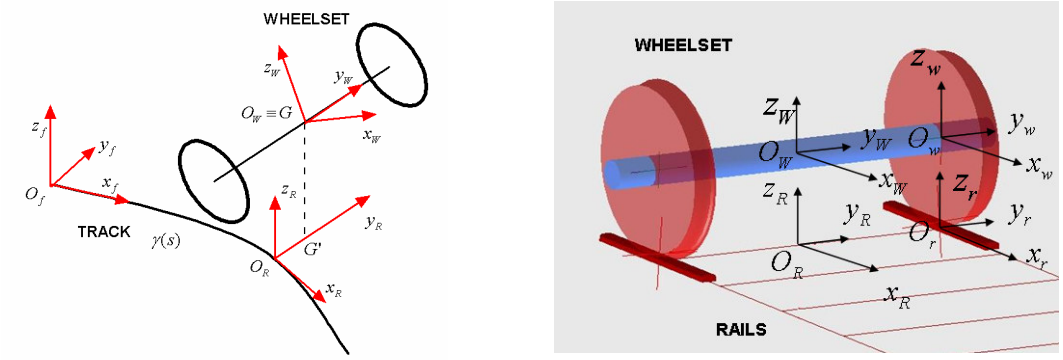


**Figure 2.** (a) Fixed, auxiliary and local systems (b) Auxiliary, local, wheel and rail systems

In order to correctly describe the differential contact model, two further reference systems have to be introduced for each wheel - rail pair: the *wheel system* $O_w x_w y_w z_w$ and the *rail system* $O_r x_r y_r z_r$. For the sake of simplicity only the left pair has been reported in Figure 2a. Both the systems are very important because the global and local contact variables will be evaluated by the contact model just in these systems. In the studied case the following standard profiles have been considered: the UIC 60 for the rails and the ORE S1002 for the wheels. [8][9][16][17][18]

## 4 THE DIFFERENTIAL WHEEL – RAIL CONTACT MODEL

In this chapter the 3D differential wheel - rail contact model will be described. For the sake of simplicity, as regards the generic contact variable $Z$, the following convention will be adopted: $Z_w$ and $Z_w^r$ will denote a variable relative to the wheel respectively expressed in the reference systems $O_w x_w y_w z_w$ and $O_r x_r y_r z_r$ while $Z_r^w$ and $Z_r$ will denote a variable relative to the rail expressed in the same systems. In the future, according to this convention, the various changes of reference system won't be continually remarked but will be taken for granted.

### 4.1 The kinematics of the problem

The wheel and the rail have been considered as two linear elastic bodies $\Omega_w$ and $\Omega_r$ (as shown in Figure 3a). Both the domains are supposed to be large enough with respect to the dimensions of the contact patch. [11][12] The boundaries $\partial\Omega_w$ and $\partial\Omega_r$ are split into two disjoint regions, respectively $\Gamma_{wC}$, $\Gamma_{wD}$ and $\Gamma_{rC}$, $\Gamma_{rD}$. The contact boundaries $\Gamma_{wC}$ and $\Gamma_{rC}$ (dashed in Figure 3a) are the regions where the contact may verify while on the Dirichlet boundaries $\Gamma_{wD}$ and $\Gamma_{rD}$ the displacements are known and equal to zero. The knowledge of the wheel - rail kinematics ($\boldsymbol{O}_w^r$, $\dot{\boldsymbol{O}}_w^r$, $R_w^r$, $\boldsymbol{\omega}_w^r$ and $\dot{\boldsymbol{O}}_r$, $\boldsymbol{\omega}_r$) and consequently of the location of the Dirichlet boundaries has been used, during the simulation, to determine the position of the undeformed configurations.

In case of contact, the geometric intersection between the surfaces $\Gamma_{wC}$ and $\Gamma_{rC}$ (and thus between the undeformed configurations) allows to define the penetration areas $\tilde{A}_{wC} \subset \Gamma_{wC}$ and $\tilde{A}_{rC} \subset \Gamma_{rC}$ (with $\tilde{A}_{wC} \simeq \tilde{A}_{rC}$) that can be considered as a first rough estimate of the real contact areas $A_{wC}$ and $A_{rC}$. The situation is schematically sketched in Figure 3b and 3c.

The real contact areas $A_{wC} \subset \tilde{A}_{wC}$ and $A_{rC} \subset \tilde{A}_{rC}$ (with $A_{wC} \simeq A_{rC}$) are unknown and have to be calculated by the model. For this purpose a contact map $\boldsymbol{\Phi}$ has to be introduced. The contact map $\boldsymbol{\Phi}: \tilde{A}_{wC} \rightarrow \tilde{A}_{rC}$ (by

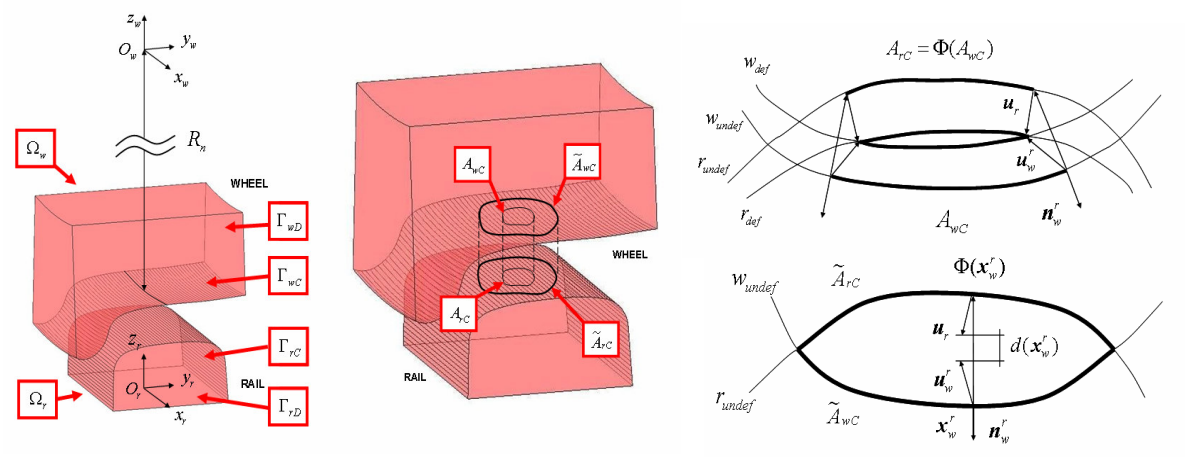


**Figure 3.** (a) Domains and boundaries (b) Contact areas (c) Contact map and distance function

convention the wheel is the master body) connects the generic point $\boldsymbol{x}_w^r \in \widetilde{A}_{wC}$ on the wheel surface with the point $\boldsymbol{\Phi}(\boldsymbol{x}_w^r) \in \widetilde{A}_{rC}$ on the rail surface that will get in contact with the point on the wheel surface in the deformed configuration. In this case the map $\boldsymbol{\Phi}$ is defined as the normal projection $\boldsymbol{\Phi}(\boldsymbol{x}_w^r)$ of the point $\boldsymbol{x}_w^r \in \widetilde{A}_{wC}$ on the surface $\widetilde{A}_{rC}$. Starting from the contact map, the distance function between the deformed configurations $d : \widetilde{A}_{wC} \to R$ can be evaluated:

$$d(\boldsymbol{x}_w^r) = \left(\boldsymbol{u}_w^r - \boldsymbol{u}_r\right) \bullet \boldsymbol{n}_w^r - \left(\boldsymbol{\Phi}(\boldsymbol{x}_w^r) - \boldsymbol{x}_w^r\right) \bullet \boldsymbol{n}_w^r \tag{1}$$

where $\boldsymbol{n}_w^r$ is the outgoing normal versor to the surfaces $\Gamma_{wC}$. The function $d$ is positive if there is penetration between the deformed configurations and negative otherwise (Figure 3c).
Formally the contact area $A_{wC}$ is defined as the region of $\widetilde{A}_{wC}$ where the function $d$ is positive while the contact area $A_{rC} = \boldsymbol{\Phi}(A_{wC})$ is the normal projection of $A_{wC}$ on $\widetilde{A}_{rC}$. In other words, from a kinematic point of view, the penetration between the deformed bodies is allowed and will have to be penalized by the contact model (see paragraph 4.2) (Figure 3c). [11][12]
In this way the estimated contact areas $\widetilde{A}_{wC}$ and $\widetilde{A}_{rC}$ depend only on the relative wheel - rail kinematics while the real contact areas $A_{wC}$ and $A_{rC}$ depend also on the displacements $\boldsymbol{u}_w$ and $\boldsymbol{u}_r$. Finally it is useful to remark that no hypothesis has been made on the shape of the contact patch; in particular, the contact area can be made up of one or more disjoint parts.

### 4.2 The contact model

According to the linear theory of elasticity [11][12], both the wheel and the rail are governed by the Navier's equations:

$$\begin{array}{llll} div\ \boldsymbol{\sigma}_w(\boldsymbol{u}_w) = \boldsymbol{0} \text{ on } \Omega_w & \boldsymbol{u}_w = \boldsymbol{0} \text{ on } \Gamma_{wD} & \boldsymbol{\sigma}_w(\boldsymbol{u}_w)\boldsymbol{n}_w = \boldsymbol{p}_w \text{ on } \widetilde{A}_{wC} & \boldsymbol{\sigma}_r(\boldsymbol{u}_r)\boldsymbol{n}_r = \boldsymbol{p}_r \text{ on } \widetilde{A}_{rC} \\ div\ \boldsymbol{\sigma}_r(\boldsymbol{u}_r) = \boldsymbol{0} \text{ on } \Omega_r & \boldsymbol{u}_r = \boldsymbol{0} \text{ on } \Gamma_{rD} & \boldsymbol{\sigma}_w(\boldsymbol{u}_w)\boldsymbol{n}_w = \boldsymbol{0} \text{ on } \Gamma_{wC} \setminus \widetilde{A}_{wC} & \boldsymbol{\sigma}_r(\boldsymbol{u}_r)\boldsymbol{n}_r = \boldsymbol{0} \text{ on } \Gamma_{rC} \setminus \widetilde{A}_{rC} \end{array} \tag{2}$$

where $\boldsymbol{n}_w$ and $\boldsymbol{n}_w$ are the outgoing normal vectors to the surfaces $\Gamma_{wC}$ and $\Gamma_{rC}$ while $\boldsymbol{p}_w$ and $\boldsymbol{p}_r$ are the unknown contact pressures. The pressures $\boldsymbol{p}_w$ and $\boldsymbol{p}_r$ are defined on $\widetilde{A}_{wC}$ and $\widetilde{A}_{rC}$ but will have to be zero on $\widetilde{A}_{wC} \setminus A_{wC}$ and $\widetilde{A}_{rC} \setminus A_{rC}$. Both the bodies have the material characteristics of the steel (Young's modulus $E_w = E_r = 2.1 * 10^{11}\, Pa$ and Poisson's coefficient $\nu_w = \nu_r = 0.3$).
In the studied case volume forces (i. e. the gravity) and inertial terms have been neglected (see Eq. 2) because their influence on the contact phenomena is very small and because they have just been considered by the multibody model of the railway vehicle. Moreover the problem is supposed to be steady within the time integration step (see Figure 1). [4][11][12]
Equivalently the problem 2 can be formulated in weak form as follows:

$$\int_{\Omega_w} \boldsymbol{\sigma}_w(\boldsymbol{u}_w) : \boldsymbol{\varepsilon}_w(\boldsymbol{v}_w) dV = \int_{\widetilde{A}_{wC}} \boldsymbol{p}_w \bullet \boldsymbol{v}_w dA \quad \forall \boldsymbol{v}_w \in V_w \qquad \int_{\Omega_r} \boldsymbol{\sigma}_r(\boldsymbol{u}_r) : \boldsymbol{\varepsilon}_r(\boldsymbol{v}_r) dV = \int_{\widetilde{A}_{rC}} \boldsymbol{p}_r \bullet \boldsymbol{v}_r dA \quad \forall \boldsymbol{v}_r \in V_r \tag{3}$$

where $\boldsymbol{\varepsilon}_w$ and $\boldsymbol{\varepsilon}_r$ are the strains while $V_w$ and $V_r$ are suitable Sobolev's spaces.

In order to complete the contact model, the contact pressures $\boldsymbol{p}_w$ and $\boldsymbol{p}_r$ have to be expressed as a function of the displacements $\boldsymbol{u}_w$ and $\boldsymbol{u}_r$. For the sake of simplicity the normal and the tangential contact pressures on the wheel are introduced: $p^r_{wN} = \boldsymbol{p}^r_w \bullet \boldsymbol{n}^r_w$, $\boldsymbol{p}^r_{wT} = \boldsymbol{p}^r_w - p^r_{wN}\boldsymbol{n}^r_w$. The normal pressure $p^r_{wN}$ has been calculated by means of the distance function $d$ and has to penalize the penetration between the deformed configurations (see paragraph 4.1):

$$p^r_{wN}(\boldsymbol{x}^r_w) = -K \max(d(\boldsymbol{x}^r_w), 0) \quad \text{on } \widetilde{A}_{wC} \tag{4}$$

where $K > 0$ is a fictitious stiffness constant. The value of $K$ has to be chosen large enough to assure the accuracy required by this kind of problems. The condition of ideal contact (total absence of penetration between the deformed configurations) is reached for $K \to +\infty$ (usually $K \geq 10^{15}$ N/m$^3$). [11][12] To evaluate the tangential pressure $\boldsymbol{p}^r_{wT}$, the slip $\boldsymbol{s}^r_w$ between the wheel and rail surfaces has to be defined. Since the solution is supposed to be steady within the integration step, the following expression holds: [4][11][12]

$$\boldsymbol{s}^r_w(\boldsymbol{x}^r_w) = \boldsymbol{w}^r_w(\boldsymbol{x}^r_w) + \dot{\boldsymbol{u}}^r_w(\boldsymbol{x}^r_w) - \boldsymbol{w}_r(\boldsymbol{\Phi}(\boldsymbol{x}^r_w)) - \dot{\boldsymbol{u}}_r(\boldsymbol{\Phi}(\boldsymbol{x}^r_w)) = \boldsymbol{w}^r_w(\boldsymbol{x}^r_w) + J^r_w(\boldsymbol{x}^r_w)\boldsymbol{w}^r_w(\boldsymbol{x}^r_w) - \boldsymbol{w}_r(\boldsymbol{\Phi}(\boldsymbol{x}^r_w)) - J_r(\boldsymbol{\Phi}(\boldsymbol{x}^r_w))\boldsymbol{w}_r(\boldsymbol{\Phi}(\boldsymbol{x}^r_w)) \tag{5}$$

where $\boldsymbol{w}^r_w$ and $\boldsymbol{w}_r$ are the rigid velocity of the points $\boldsymbol{x}^r_w$ and $\boldsymbol{\Phi}(\boldsymbol{x}^r_w)$ (computable starting from the knowledge of the wheel - rail kinematic variables) while $J^r_w$ and $J_r$ are the Jacobians of $\boldsymbol{u}^r_w$ and $\boldsymbol{u}_r$ with respect to the variables $\boldsymbol{x}^r_w$ and $\boldsymbol{x}_r$. As usual the normal and the tangential slips are: $s^r_{wN} = \boldsymbol{s}^r_w \bullet \boldsymbol{n}^r_w$, $\boldsymbol{s}^r_{wT} = \boldsymbol{s}^r_w - s^r_{wN}\boldsymbol{n}^r_w$. According to the standard pseudo – coulombian friction models, the tangential pressures $\boldsymbol{p}^r_{wT}$ can be expressed as follows:

$$\boldsymbol{p}^r_{wT}(\boldsymbol{x}^r_w) = -\mu(\| \boldsymbol{s}^r_{wT}(\boldsymbol{x}^r_w) \|, V) \left| p^r_{wN}(\boldsymbol{x}^r_w) \right| \boldsymbol{s}^r_{wT}(\boldsymbol{x}^r_w) / \| \boldsymbol{s}^r_{wT}(\boldsymbol{x}^r_w) \| \quad \text{on } \widetilde{A}_{wC} \tag{6}$$

where $V$ is the longitudinal velocity of the vehicle. Further details on the friction function $\mu(\| \boldsymbol{s}^r_{wT} \|, V)$ can be found in the literature. [4][11][12][17] Finally the action – reaction principle (the Newton's Third Law) allows to calculate the pressures $\boldsymbol{p}_r$: $\boldsymbol{p}_r(\boldsymbol{\Phi}(\boldsymbol{x}^r_w)) = -\boldsymbol{p}^r_w(\boldsymbol{x}^r_w)$ on $\widetilde{A}_{wC}$. In conclusion It is useful to remark that, according to the described model, the contact pressures $\boldsymbol{p}^r_w$ and $\boldsymbol{p}_r$ are zero respectively on $\widetilde{A}_{wC} \setminus A_{wC}$ and $\widetilde{A}_{rC} \setminus A_{rC}$. The displacements $\boldsymbol{u}_w$ and $\boldsymbol{u}_r$ will be evaluated in the following through the numerical solution of Eq. 3. The knowledge of these unknown quantities will allow to calculate all the other required outputs like the contact areas $A_{wC}$ and $A_{rC}$ and the stresses $\sigma_w$ and $\sigma_r$. The contact forces $\boldsymbol{F}_{wC}$ and $\boldsymbol{F}_{rC}$ will be estimated by integration: $\boldsymbol{F}_{wC} = \int_{\widetilde{A}_{wC}} \boldsymbol{p}_w dA$, $\boldsymbol{F}_{rC} = \int_{\widetilde{A}_{rC}} \boldsymbol{p}_r dA$.

### 4.3 The discretization of the model

Both the elastic bodies have been discretized by means of tetrahedral elements and linear shape functions. The meshes have been built according to the standard Delaunay's algorithms (see Figure 4). [13][14]
The resolution of the meshes on the surfaces $\Gamma_{wC}$ and $\Gamma_{rC}$ is constant because the position and the dimensions of the contact area are a priori unknown. Moreover the surface resolution (usually in the range $0.1\text{mm} \div 1.0\text{mm}$) has to assure an accuracy enough to correctly describe the contact phenomena. It is important to remark that the meshes have been created directly in the reference systems $O_w x_w y_w z_w$ and $O_r x_r y_r z_r$; therefore they don't change during the simulation and can be easily built offline without increasing the computational load.
The knowledge of the wheel - rail kinematics and consequently of the estimated contact areas $\widetilde{A}_{wC}$ and $\widetilde{A}_{rC}$ allows to determine the sets $C_w$ and $C_r$ of the active contact elements on the wheel and on the rail.For each active contact element on the wheel, the center $\boldsymbol{x}^r_{w\,i}$ of the face $\widetilde{A}^i_{wC}$ is considered. The normal projection $\boldsymbol{x}_{r\,j} = \boldsymbol{\Phi}(\boldsymbol{x}^r_{w\,i})$ of $\boldsymbol{x}^r_{w\,i}$ on $\widetilde{A}_{rC}$ will belong to the external face $\widetilde{A}^j_{rC}$ of the $j$-th active contact element on the rail; in particular the index $j(i)$ will be a function of the index $i$. In this way the pairs of points $(\boldsymbol{x}^r_{wi}, \boldsymbol{x}_{rj(i)})$ with $i \in C_w$ can be thought of as the discretization of the contact map $\boldsymbol{\Phi}$. The situation is schematically sketched in Figure 4. The values of the displacements $\boldsymbol{u}^r_w$, $\boldsymbol{u}_r$ of their Jacobians $J^r_w$, $J_r$ in the points $\boldsymbol{x}^r_{w\,i}$, $\boldsymbol{x}_{r\,j}$ are evaluated through the shape functions. [11][12][13][14]

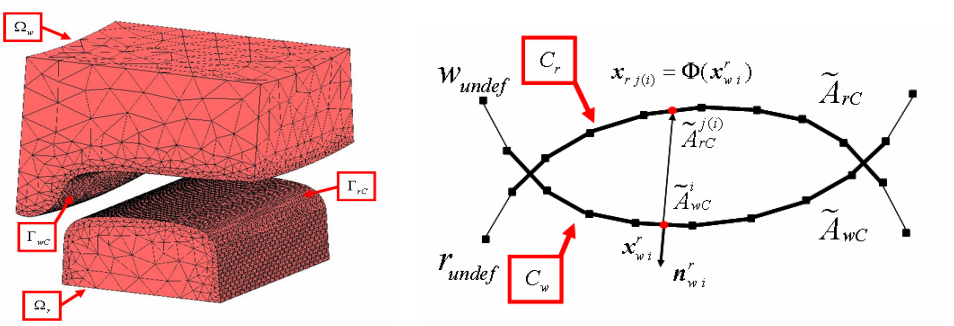


**Figure 4.** Discretization of the contact model

At this point the distance function $d_i = d(\boldsymbol{x}^r_{w\,i})$ and the pressure $\boldsymbol{p}^r_{w\,i} = \boldsymbol{p}^r_w(\boldsymbol{x}^r_{w\,i})$ on the face $\tilde{A}^i_{wC}$ of the active element of the wheel can be calculated by means of Eq. 1, 4 and 6. Finally a discrete version of the action - reaction principle (the Newton's Third Law) is needed to evaluate the pressure $\boldsymbol{p}_{r\,j(i)} = \boldsymbol{p}_r(\boldsymbol{x}_{r\,j(i)})$ on the face $\tilde{A}^{j(i)}_{rC}$ of the active element of the rail: $|\tilde{A}^{j(i)}_{rC}|\,\boldsymbol{p}_{r\,j(i)} = -|\tilde{A}^i_{wC}|\,\boldsymbol{p}^r_{w\,i}$.

Standard FEM techniques allow to discretize the weak form of the contact problem (see Eq. 3) as follows: [11][12][13][14]

$$K_w \boldsymbol{U}_w = \boldsymbol{F}_w(\boldsymbol{U}_{wC}, \boldsymbol{U}_{rC}) \quad K_r \boldsymbol{U}_r = \boldsymbol{F}_r(\boldsymbol{U}_{wC}, \boldsymbol{U}_{rC})\,. \tag{7}$$

The global stiffness matrices $K_w$ and $K_r$ are symmetric, positive defined and sparse; $\boldsymbol{U}_w$, $\boldsymbol{U}_r$ comprise the displacements relative to all the nodes of wheel and rail while $\boldsymbol{U}_{wC}$ and $\boldsymbol{U}_{rC}$ only the displacements relative to the active elements. Moreover $K_w$ and $K_r$ are evaluated directly in the reference systems $O_w x_w y_w z_w$ and $O_r x_r y_r z_r$; therefore they don't change during the simulation and can be easily built offline without increasing the computational load. Eq. 7 will be called the *sparse formulation* of the discrete contact problem. This equation can be also written as $\boldsymbol{U}_w = H_w \boldsymbol{F}_w(\boldsymbol{U}_{wC}, \boldsymbol{U}_{rC})$, $\boldsymbol{U}_r = H_r \boldsymbol{F}_r(\boldsymbol{U}_{wC}, \boldsymbol{U}_{rC})$ where the matrices $H_w$ and $H_r$ are symmetric, positive defined and full. Like $K_w$ and $K_r$ they don't change during the simulation and can be calculated offline (however their storage can require an high memory consumption). Splitting $\boldsymbol{U}_w$, $\boldsymbol{U}_r$ into contact displacements $\boldsymbol{U}_{wC}$, $\boldsymbol{U}_{rC}$ and non - contact displacements $\boldsymbol{U}_{wNC}$, $\boldsymbol{U}_{NC}$, the following relations can be obtained

$$\begin{pmatrix} \boldsymbol{U}_{wNC} \\ \boldsymbol{U}_{wC} \end{pmatrix} = \begin{bmatrix} H_w^{11} & H_w^{12} \\ H_w^{21} & H_w^{22} \end{bmatrix} \begin{pmatrix} \boldsymbol{0} \\ \boldsymbol{f}_w(\boldsymbol{U}_{wC}, \boldsymbol{U}_{rC}) \end{pmatrix} \quad \begin{pmatrix} \boldsymbol{U}_{rNC} \\ \boldsymbol{U}_{rC} \end{pmatrix} = \begin{bmatrix} H_r^{11} & H_r^{12} \\ H_r^{21} & H_r^{22} \end{bmatrix} \begin{pmatrix} \boldsymbol{0} \\ \boldsymbol{f}_r(\boldsymbol{U}_{wC}, \boldsymbol{U}_{rC}) \end{pmatrix}. \tag{8}$$

In this way the second and the fourth components of Eq. 8 are sufficient to calculate the contact displacements $\boldsymbol{U}_{wC}$, $\boldsymbol{U}_{rC}$:

$$\boldsymbol{U}_{wC} = H_w^{22} \boldsymbol{f}_w(\boldsymbol{U}_{wC}, \boldsymbol{U}_{rC}) \quad \boldsymbol{U}_{rC} = H_r^{22} \boldsymbol{f}_r(\boldsymbol{U}_{wC}, \boldsymbol{U}_{rC})\,. \tag{9}$$

Eq. 9 will be called the *reduced formulation* of the discrete contact problem. The matrices $H_w^{22}$ and $H_r^{22}$ have the same properties as $H_w$ and $H_r$ but this time their dimensions are much smaller. However $H_w^{22}$ and $H_r^{22}$ change during the simulation and therefore have to be built directly online.

The knowledge of the displacements $\boldsymbol{U}_w$, $\boldsymbol{U}_r$, evaluated by solving Eq. 7 or Eq. 9, allows to calculate all the other required outputs like the contact areas $A_{wC}$ and $A_{rC}$ and the stresses $\sigma_w$ and $\sigma_r$. The contact forces $\boldsymbol{F}_{wC}$ and $\boldsymbol{F}_{rC}$ are estimated by numerical integration: $\boldsymbol{F}_{wC} = \sum_{i \in C_w} |\tilde{A}^i_{wC}|\,\boldsymbol{p}_{w\,i}$, $\boldsymbol{F}_{rC} = \sum_{i \in C_w} |\tilde{A}^{j(i)}_{rC}|\,\boldsymbol{p}_{r\,j(i)}$.

### 4.4 The numerical solution of the discrete problem

In this paragraph the numerical methods used for solving the discrete contact problem are presented. Both the *sparse formulation* (Eq. 7) and the *reduced formulation* (Eq. 9) will be analyzed in the following. Eq. 7 is a large and sparse nonlinear system; on the contrary Eq. 9 is a full non linear system with much smaller dimensions than 7. The typical dimensions of $K_w$ and $K_r$ (depending on the mesh resolution) are in the range $10^4 \div 10^5$ while those of $H_w^{22}$ and $H_r^{22}$ (depending on the number of active elements) are about $10^2 \div 10^3$.

Nonlinear solvers based on Newton - Krylov methods are usually very efficient for solving large and sparse systems like Eq. 7. [19] Newton - Krylov methods are Newton-type methods for the problem $\boldsymbol{F}(\boldsymbol{x})=\boldsymbol{0}$ where $\boldsymbol{F}$ is a generic nonlinear function. In particular, Krylov methods are employed to solve approximately the arising linear systems: $F'(\boldsymbol{x}_k)\boldsymbol{s}_k=-\boldsymbol{F}(\boldsymbol{x}_k)$ where $F'$ is the Jacobian of $\boldsymbol{F}$. The Krylov method computes, at each iteration, the so-called inexact Newton step $\tilde{\boldsymbol{s}}_k$ which satisfies the condition $\|F'(\boldsymbol{x}_k)\tilde{\boldsymbol{s}}_k+\boldsymbol{F}(\boldsymbol{x}_k)\|\le\eta_k\|\boldsymbol{F}(\boldsymbol{x}_k)\| \quad \eta_k\in[0,1)$ where the forcing terms $\eta_k$ are used to control the level of accuracy. [19] In the studied case a constant forcing term $\eta_k=\eta\le 0.5 \ \forall k$ has been chosen while the method stops if the following stopping criterion is satisfied: $\|\boldsymbol{F}(\boldsymbol{x}_k)\|<Tol$. As regards the considered problem, numerical experimentations showed that, among all the Krylov methods, the best linear solver is the BiCGStab. [20] This particular kind of nonlinear solver is known as Newton - BiCGStab method.
Iterative methods like the BiCGStab need often a good preconditioner. The employed preconditioner $P$ has been defined as follows: $P=diag(K_w,K_r)$. Since Eq. 7 is weakly nonlinear, the preconditioner $P$ is a good approximation of the Jacobian. In general, the BiCGStab does not require the whole matrix $P$ but only a factorization of it. In the considered case the incomplete Cholesky factorization [20] has been used because the matrix $P$ is not only symmetric and positive defined but also sparse. Moreover this factorization performs a reordering of $P$ and takes advantage of its sparsity in terms of execution time and memory consumption.
An interesting feature of the Newton - BiCGStab method is that it requires only the action of $F'$ on a vector $\boldsymbol{v}$ but not the computation and the storage of the whole Jacobian. In this case, the product $F'(\boldsymbol{x})\boldsymbol{v}$ can be approximated by means of finite differences: $F'(\boldsymbol{x})\boldsymbol{v}\simeq(\boldsymbol{F}(\boldsymbol{x}+\varepsilon\boldsymbol{v})-\boldsymbol{F}(\boldsymbol{x}))/\varepsilon$ where $\varepsilon>0$ is a scalar small enough. [21] Consequently this method is called "matrix free".
The same nonlinear solver (Newton - BiCGStab), this time without preconditioner, has been used in order to solve Eq. 9. In this circumstance, due to the small dimensions of the problem, the arising linear systems can be also solved by means of direct methods (like the LU method [22]). Therefore a second nonlinear solver based on this kind of procedures (the Newton - LU method) has been analyzed and experimented on the system 9. The employment of this alternative approach needs the computation and the storage of the whole Jacobian $F'$ at each nonlinear iteration.
Finally, it has to be remarked that, if the guarantee of convergence is only local, the nonlinear solvers (the Newton - BiCGStab and the Newton - LU) may fail in finding a solution, even though an effective solution exists. Therefore both the numerical procedures have been embedded into a globalization strategy. A monotone line search method with Armijo rule has been employed, with a maximum of 10 backtracks for nonlinear iteration. [21][22]
As regards the time integration of the whole model (multibody model and contact model; see Figure 1), explicit ODE solvers with variable step and variable order have been considered. [23] Moreover, during the simulations, the initial conditions for the nonlinear solvers (the Newton - BiCGStab and the Newton - LU) are continually updated in order to speed up the convergence of the solvers and to reduce the computation time. In other words the solution of the problem at the current time step is used as initial condition for the solver at the next time step.

## 5 THE MULTIBODY MODEL

As benchmark vehicle the Manchester Wagon has been chosen (see Figure 5a); the physical and geometrical characteristics of the vehicle can be found in literature. [5][15] The multibody model consists of seven rigid bodies: the car body, two bogies and four wheelsets. The secondary suspensions connect the bogies to the car body while the primary suspensions connect the wheelsets to the bogies. Both the stages of suspensions have been modelled by means of three-dimensional viscoelastic force elements (linear and nonlinear). The multibody model of the Manchester Wagon has been implemented in SimMechanics, a Matlab toolbox specifically designed for the multibody dynamics.

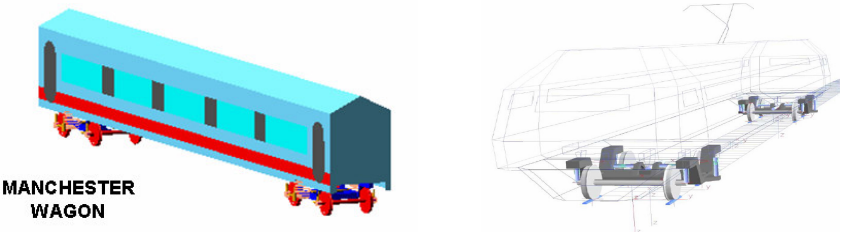


**Figure 5.** (a) Matlab multibody model (b) Simpack Rail multibody model

The 3D multibody model of the same vehicle has been then implemented also in Simpack Rail, a commercial multibody software for railway vehicles widely tested and validated (Figure 5b). [15] This time the model is equipped with a standard contact model based on the semi - elastic approach and able to consider the multiple contact (see the introduction). [4][5][6][7][8][9] The comparison between the results obtained by the Matlab model and those obtained by the Simpack Rail model has allowed an accurate and reliable validation of the new contact model.

## 6 THE NUMERICAL SIMULATIONS

With the aim of studying the behavior of the whole model (see Figure 1), a large number of dynamic simulations has been performed on many different sceneries obtained by varying the geometrical characteristics of the railway track. [5][15][16] By way of example a typical simulation of the dynamics of the Manchester Wagon will be considered. The simulation has been carried out on a curvilinear railway track, the data of which are reported in Table 1a (on a machine provided with an Intel Xeon 2.66GHz and 8GB RAM). [5][15][16]

| | | |
|---|---|---|
| Curvature | $K$ | -1/1200 $m^{-1}$ |
| Slope | $p$ | 0 |
| Cant | $\beta$ | 0.0418 rad |
| Laying angle | $\alpha_p$ | 1/40 rad |
| Velocity | $V$ | 162 km/h |
| Friction coefficient | $\mu$ | 0.3 |

| Contact Model | Eq. 7 | Eq. 9 | Eq. 9 |
|---|---|---|---|
| RelTol / AbsTol | $10^{-8}$ / $10^{-6}$ | $10^{-8}$ / $10^{-6}$ | $10^{-8}$ / $10^{-6}$ |
| Nonlinear Solver | Newton-BiCGStab | Newton-BiCGStab | Newton-LU |
| Tol / MaxitNonlin | $10^{-7}$ / 20 | $10^{-7}$ / 20 | $10^{-7}$ / 20 |
| $\eta$ / MaxitLin | 0.01 / 20 | 0.01 / 20 | - |

**Table 1.** (a) Data of the curvilinear track (b) Numerical parameters

First of all, in order to compare the *sparse formulation* 7 and the *reduced formulation* 9 of the contact problem, several experimentations have been performed with different ODE solvers like the ODE23 and the ODE45. [23] The values of the main numerical parameters relative to the simulation are reported in Table 1b for both the formulations.
The results showed that the *reduced formulation* 9 is more efficient than the *sparse formulation* 7 even though the *reduced formulation* 9 may require a bigger memory consumption (see paragraph 4.3). In both cases ODE solvers with low order like the ODE23 turned out to be faster than ODE solvers with higher order like the ODE45.
Table 2 summarizes, for instance, the results obtained by using the ODE 23 and relative to the *reduced formulation* 9. For each wheel - rail contact pair the following data have been considered: (1) the number $CPS$ of contact problems solved during the dynamic simulation (equal for all the eight contact pairs); (2) the mean computation times $CT$ relative to each contact model (the time needed to solve one contact problem) and the total computation time required by the eight contact models; (3) the total number $IterNonlin$ of nonlinear iterations and the convergence errors of the nonlinear solver $ErrorNonlin$; (4) the total number $IterLin$ of linear iterations and the convergence errors of the linear solver $ErrorLin$.

| **Differential Contact Model: *Reduced Formulation* 9** | | | | | | |
|---|---|---|---|---|---|---|
| **Wheel – Rail Pair** | *CPS* | *CT* $3^h\ 46^m$ | *IterNonlin* | *ErrorNonlin* | *IterLin* | *ErrorLin* |
| 1° Wheelset (Left Wheel) | 150156 | 12.0 ms | 162111 | 13 | 705742 | 1428 |
| 1° Wheelset (Right Wheel) | 150156 | 10.7 ms | 148925 | 4 | 609546 | 787 |
| 2° Wheelset (Left Wheel) | 150156 | 12.0 ms | 160709 | 3 | 757143 | 1659 |
| 2° Wheelset (Right Wheel) | 150156 | 10.6 ms | 148501 | 9 | 643307 | 705 |
| 3° Wheelset (Left Wheel) | 150156 | 12.1 ms | 163581 | 4 | 755329 | 1410 |
| 3° Wheelset (Right Wheel) | 150156 | 10.5 ms | 147231 | 5 | 629624 | 928 |
| 4° Wheelset (Left Wheel) | 150156 | 12.3 ms | 162085 | 4 | 792693 | 1368 |
| 4° Wheelset (Right Wheel) | 150156 | 10.3 ms | 144923 | 7 | 626424 | 666 |

**Table 2.** Performance of the *reduced formulation* 9 using the ODE23

As said in the paragraph 4.4, the *reduced formulation* 9 has been also solved by means of the Newton - LU nonlinear solver. The used ODE solver is the ODE23 while the values of the main numerical parameters relative to the simulation are reported in table 1b. In this case the comparison between the results showed that the Newton - BiCGStab method is more efficient than the Newton - LU method in spite of the small dimensions of the discrete problem 9 (the *reduced formulation*). In particular the computation and the storage of the whole Jacobian at each nonlinear iteration turn out to be quite time - consuming.
Among all the outputs evaluated by the models (kinematic variables, internal forces, contact forces and contact areas), for the sake of simplicity only the time histories of the following quantities have been

reported: the lateral displacement $y_W^R$ of the center of mass and the roll angle $\varphi_W^R$ of the first wheelset (in the system $O_R x_R y_R z_R$; blue for Matlab and red for Simpack Rail, see Figure 6a and 6b), the lateral $Y_{lw}^R$ and vertical $Q_{lw}^R$ resultant contact forces on the left wheel of the wheelset (in the system $O_R x_R y_R z_R$; blue for Matlab and red for Simpack Rail, see Figure 7a and 7b) and the real contact areas $A_{wlC}$, $A_{rlC}$ on the left wheel and rail surfaces (respectively expressed in the systems $O_W x_W y_W z_W$ and $O_R x_R y_R z_R$; blue for Matlab and black for Simpack Rail, see Figure 8a and 8b). In order to give a clear and effective description of the motion of the contact areas calculated by the Matlab model, a lateral section of the contact patches has been plotted on cylindrical surfaces obtained from the wheel and rail profiles (generating profiles) and as long as the distance travelled by the vehicle. Concerning the Simpack Rail model (equipped with a standard contact model), the position of the contact points has been plotted.

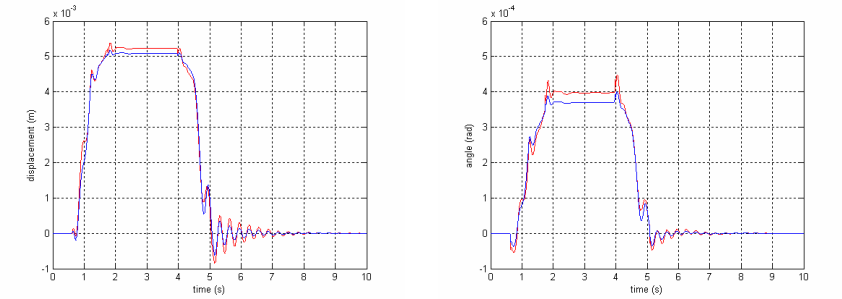


**Figure 6.** (a) Wheelset: lateral displacement of the center of mass (b) Wheelset: roll angle

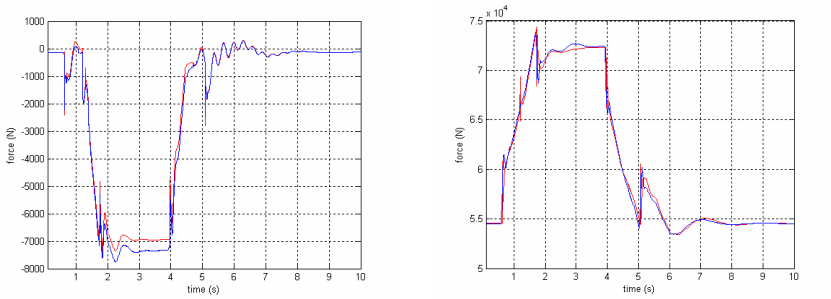


**Figure 7.** (a) Lateral contact force on the left wheel (b) Vertical contact force on the left wheel

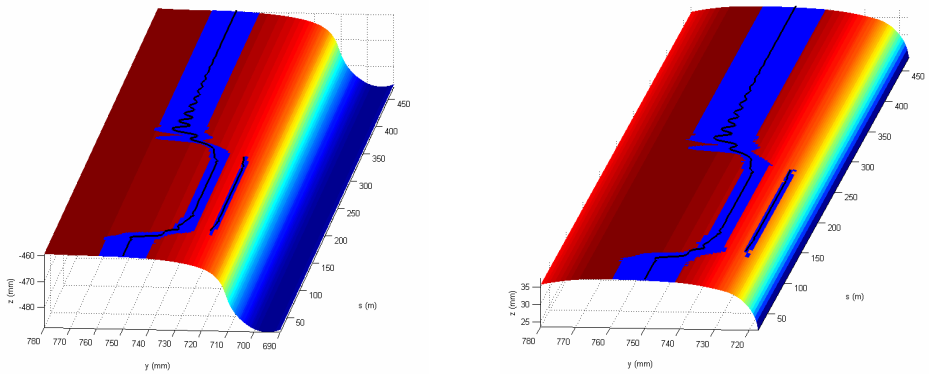


**Figure 8.** (a) Section of the contact area on the left wheel (b) Section of the contact area on the left rail

The analysis of the results shows a good agreement between the Matlab and the Simpack Rail model both in terms of kinematic variables and in terms of resultant contact forces. Moreover, during the curve, the contact areas calculated by the Matlab model on the left wheel and rail surfaces are made up of two disjoint parts (in other words a multiple contact is present). On the other hand, also the Simpack Rail model detects, during the curve, the presence of a second contact point on the left wheel and rail; in particular the contact points are always contained within the different disjoint parts of the contact areas estimated by the Matlab model. From this point of view there is a good agreement between the models.
In conclusion it is usefull to observe as the stability of the Matlab model and the quasi – total absence of numerical noise highlight the accuracy and the reliability of the new contact model.

## 7 CONCLUSIONS

In this work the authors presented an innovative elastic wheel - rail contact model with the aim of achieving a better integration between multibody and differential modeling. Due to the high computational load, this kind of integration is almost absent in literature especially in the railway field; however it is very important because only the differential modeling allows an accurate analysis of the contact phenomena while the multibody modeling is the standard in the study of the railway dynamics.
The performances of the Matlab model turned out to be good both in terms of output accuracy (kinematic variables, contact forces and contact areas) and in terms of numerical efficiency (performances of the numerical algorithms and time consumption) and satisfy all the specifics reported in the introduction.

## REFERENCES


[1] SHABANA, A. A. AND SANY, J. R. An augmented formulation for mechanical systems with non-generalized coordinates. *Nonlinear Dynamics 24*, (2001), 183 – 204.

[2] IWNICKI, S. Simulation of wheel – rail contact forces. *Fatigue and Fracture of Engineering Materials and Structures 26*, (2003), 887 – 900.

[3] POMBO, J. AND AMBROSIO, J. Dynamic analysis of a railway vehicle in real operation conditions using a new wheel – rail contact detection model. *International Journal of Vehicle Systems Modelling and Testing 1*, (2005), 79 – 105.

[4] KALKER, J. J. *Three – dimensional Elastic Bodies in Rolling Contact*, Kluwer Academic Publishers, Dordrecht, Netherlands, 1990.

[5] DUKKIPATI, R. V. AND AMYOT, J. R. *Computer Aided Simulation in Railway Dynamics*, Dekker, New York, 1988.

[6] POLACH, O. Creep forces in simulations of traction vehicles running on adhesion limit. *Wear 258*, (2005), 992 – 1000.

[7] SHABANA, A. A., ZAAZAA, K. E. ET AL. Development of elastic force model for wheel/rail contact problems. *Journal of Sound and Vibration 269*, (2004), 295 – 325.

[8] FALOMI, S., MALVEZZI, M., MELI, E. AND RINDI, A. Determination of wheel – rail contact points with semianalytic methods. *Multibody System Dynamics 20*, 4 (2008), 327 – 358.

[9] AUCIELLO, J., FALOMI, S., MALVEZZI, M. AND MELI, E. Dynamic simulation of railway vehicles: wheel – rail contact analysis. *Vehicle System Dynamics 47,* 7 (2009), 867-899.

[10] JOHNSON, K. L. *Contact Mechanics*, Cambridge University Press, Cambridge, England, 1985.

[11] KIKUCHI, N. AND ODEN, J. T. *Contact Problems in Elasticity*, SIAM Studies in Applied Mathematics, Philadelphia, Pennsylvania, 1988.

[12] WRIGGERS, P. *Computational Contact Mechanics*, Wiley & Sons, Hoboken, New Jersey, 2002.

[13] ZIENKIEWICZ, O. *The Finite Element Method in Engineering Science*, McGraw – Hill, New York, 1988.

[14] DHATT, G. AND TOUZOT, G. *The Finite Element Method Displayed*, Wiley & Sons, Hoboken, New Jersey, 1984.

[15] IWNICKI, S. *The Manchester Benchmarks for Rail Vehicle Simulators*, Swets & Zeitlinger, Lisse, Netherlands, 1999.

[16] ESVELD, C. *Modern Railway Track*, Delft University of Technology, Delft, Netherlands, 2001.

[17] VICUNA, G. *Organizzazione e Tecnica Ferroviaria*, Ed. CIFI, Roma, Italy, 1986.

[18] DO CARMO, M. *Geometry of Curves and Surfaces*, Prentice Hall, Upper Saddle River, New Jersey, 1976.

[19] DEMBO, R. S, EISENSTAT, S. C. AND STEIHAUG, T. Inexact Newton methods. *SIAM Journal of Numerical Analysis* 19, (1982), 400 – 408.

[20] KELLEY, C. T. *Iterative Methods for Linear and Nonlinear Equations*, SIAM, Philadelphia, Pennsylvania, 1995.

[21] SAAD, Y. *Iterative Methods for Sparse Linear Systems*, SIAM, Philadelphia, Pennsylvania, 2003.

[22] NOCEDAL, J. AND WRIGHT, S. J. *Numerical Optimization*, Springer Series in Operation Research, Berlin, Germany, 1999.

[23] SHAMPINE, L. F. AND REICHELT, M. W. The MATLAB ODE Suite. *SIAM Journal on Scientific Computing* 18, (1997), 1 – 22.